Acta Materialia 124 (2017) 468–477

Contents lists available at ScienceDirect

Acta Materialia

journal homepage: www.elsevier.com/locate/actamat

Full length article

# Surface excess elasticity of gold: Ab initio coefficients and impact on the effective elastic response of nanowires

B.A.M. Elsner [a, *], S. Müller [a], S. Bargmann [b], J. Weissmüller [c, d]

[a] Institute of Advanced Ceramics, Hamburg University of Technology, Germany
[b] Chair of Solid Mechanics, University of Wuppertal, Germany
[c] Institute of Materials Research, Materials Mechanics, Helmholtz-Zentrum Geesthacht, Germany
[d] Institute of Materials Physics and Technology, Hamburg University of Technology, Germany

ARTICLE INFO

*Article history:*
Received 25 April 2016
Received in revised form
10 October 2016
Accepted 25 October 2016
Available online 20 November 2016

*Keywords:*
Surface excess elastic parameters
Surface Lamé constants
Nanoelasticity
Nanowire
Density functional theory

ABSTRACT

Predicting the influence of the surface on the effective elastic properties of nanoscale structures and nanomaterials remains a challenge, which we here address on both levels, continuum and atomic. Density Functional Theory (DFT) computation at the atomic level yields the first reliable surface excess elastic parameters for the (111) and (001) surfaces of gold. At the continuum level, we derive closed-form expressions for the effective elastic behavior that can be combined with the DFT-derived excess elastic parameters to obtain the effective axial, torsion, and bending stiffness of circular nanowires with surface excess elasticity. The two approaches use different reference frames, and we emphasize the need for consistent stress definitions and for conversion between the separate stress measures when transferring results between the approaches. We present excess elastic parameters separately for Cauchy and 2nd Piola-Kirchhoff stresses, demonstrating that the conversion substantially modifies their numerical value and may even invert their sign. The results afford an assessment of the contribution of the surface excess elastic parameters to the effective elastic response of nanoscale beams or wires. This assessment sheds doubt on earlier suggestions relating experimental observations of an effective stiffening or softening at small size to the excess elasticity of clean surfaces.
© 2016 Acta Materialia Inc. Published by Elsevier Ltd. This is an open access article under the CC BY-NC-ND license (http://creativecommons.org/licenses/by-nc-nd/4.0/).

## 1. Introduction

The size-dependent elastic response of nanomaterials and nanostructures is of great interest in a variety of nano-electromechanical systems, such as ultrahigh-frequency nanowire resonators [1–4] or nanoporous metal actuators [5,6]. However, experimental evidence concerning the magnitude and direction of this size effect remains contradictory: With a decrease of the characteristic dimension, some experiments find an enhanced stiffness [7–11] while others point towards enhanced compliance [12,13]. The large experimental uncertainty is emphasized by studies which report both, stiffening and softening, for the same material [14].

The local elasticity of surfaces has been proposed as a key factor regarding the origin of the size-dependent effective properties [3,7,8]. A quantitative measure of this local elastic response is provided by the surface excess elastic parameters, which are defined through the response of surface stress to tangential strain at the surface [15].

In view of contradictory experimental results on magnitude and sign of the excess elastic parameters, studies of nanoporous gold (NPG), a material that can be understood as a network of nanoscale struts or 'ligaments', are remarkable: The effective elasticity of the material varies if the pore surfaces are wetted by electrolyte and the electrode potential is modulated. The finding confirms unambiguously that surface excess elasticity contributes significantly to the overall elastic response [6]. Furthermore, two independent studies report in the order of tenfold stiffening of NPG as the ligament size decreased [9,11]. This may suggest positive-valued excess elastic parameters, yet the suggestion is controversial [11], and indeed little size-dependence is found for Au nanowires [16]. It is also noteworthy that several studies emphasize the role of nonlinear elasticity at small size, specifically in metal multilayers [17] and in nanowires [2,10,18]. The reasoning is that nanoscale objects are pre-strained by the action of the surface stresses and may thus probe bulk nonlinear elastic behavior. The surface-induced strain in

* Corresponding author.
*E-mail address:* beatrix.elsner@tuhh.de (B.A.M. Elsner).

http://dx.doi.org/10.1016/j.actamat.2016.10.066
1359-6454/© 2016 Acta Materialia Inc. Published by Elsevier Ltd. This is an open access article under the CC BY-NC-ND license (http://creativecommons.org/licenses/by-nc-nd/4.0/).

a nanowire includes shear components [19], and this may lead to substantial shear softening or even shear instability of the bulk [20]. Such higher-order elasticity effects are not readily separated from surface excess elasticity in experiment.

Atomistic numerical analysis allows to explore surface excess elasticity in isolation. Models based on the Embedded Atom Method (EAM) tend to predict an enhanced compliance [2], and negative-valued surface excess elastic parameters have been reported in EAM studies of various metallic surfaces [21,22]. However, it has not been established that EAM potentials provide a valid probe of surface excess elasticity. In fact, the more substantiated Density Functional Theory (DFT) studies of the effective elastic response of thin films or nanowires disagree with the EAM-derived trends by allowing for stiffening in certain crystallographic orientations [23]. While numerical values are available for ZnO [24,25], GaN [25], and AlN [25,26], no DFT data for metals has been reported so far.

To summarize, experiments support surface excess elasticity but fail to establish its magnitude or even the sign. Excess elastic parameters have been reported based on EAM potentials, but the numerical values or signs derived from such studies lack a solid physical basis. DFT can provide more substantiated insights, but application of this technique to surface elasticity is computationally extremely demanding, and in fact DFT-based excess elastic parameters for metallic surfaces have not yet been reported. This, alongside the increase of available computational resources, motivates our study to this matter.

Linking the surface excess elastic parameters to experimentally observable effects such as, for instance, the elasticity of nanowires, requires a continuum theory for the effective elastic behavior. Of interest in relation to small-scale axial tension tests on nanowires (see e.g. [10]) is the effective Young's modulus. Cantilever resonators deform in bending, and thus results for the effective bending stiffness are needed. NPG can be modeled as a network of nanoscale struts which may predominantly deform in either, tension or bending and torsion, depending on the solid fraction [27]. This emphasizes the interest in effective values of axial, bending, and torsion stiffness.

Here, we derive closed-form expressions for the effective stiffness of a nanowire under different loading conditions in a form that supports direct insertion of the DFT-derived surface elastic parameters. We combine a continuum analysis with a DFT study into the surface elastic parameters for Au(111) and (001) as the basis for discussing the impact of surface excess elasticity on the effective stiffness of nanoscale structures.

In the following Section and throughout the discussion, we emphasize the requirement of a seamless connection between both approaches in terms of the employed variables. The discussion highlights how the surface stress and surface excess elastic parameters are affected by the frame of reference, stressing the need for consistency between the applied methods.

## 2. Connecting theory and experiment: reference frames, stress definitions, and locating the dividing surface

We wish to predict the experimental signature of the size-dependent elastic response of nanostructures based on an ab initio analysis of the atomic-scale interaction at crystal surfaces. Our analysis of the elasticity of nanowires in the framework of continuum mechanics provides the link between the local elastic response at the surface, which emerges from our DFT computation, and the effective elastic response of the nanoscale object, which is observed experimentally. Each of the above approaches—experiment, DFT, continuum theory—turns out to naturally connect to its individual set of definitions of stress, strain, and spacial reference frame. Accounting consistently for these definitions is quintessential for a correct handshake between the approaches. This theme is outlined in the following.

The database of a typical experiment, for instance a tensile test on a nanowire, comprises the initial (before loading) length and cross-section of the sample, plus the length change and the net load in each state of deformation. The effective Young's modulus is computed as the slope in a plot of “engineering stress” versus “engineering strain”, that is, of physical load per initial cross-section versus length change per initial length. In the language of continuum mechanics, referring stress and strain to the initial geometry means that “Lagrangian” coordinates are used, and the ratio of physical load over referential cross-section is a component of what is termed the $1^{st}$ *Piola-Kirchhoff* stress **P**.

In continuum theory it is often more convenient to work with different measures for stress and strain that, contrary to **P**, warrant a representation by symmetric tensors. Our work adopts one such approach, which underlies standard studies of surface elasticity. Here, free energy changes are derived from the $2^{nd}$ *Piola-Kirchhoff* stress **S** and the Lagrangian (or Green) strain as the two energy-conjugate quantities.

The DFT computation requires yet another stress measure: Individual simulations are not aware of the concept of an undeformed reference configuration, and hence the stress is computed as load per area of the actual, deformed configuration [28,29]. This is the so-called *Cauchy* stress $\boldsymbol{\sigma}$. The definitions of and conversions between the various stress measures are well established, see e.g. the textbook by Bonet and Wood [30]. Throughout our derivation, we shall keep the reader aware of these distinctions and their implications for comparing theory and experiment.

Our analysis of elastic deformation is based on a smooth displacement vector function $\mathbf{u}(\mathbf{X})$ with $\mathbf{X}$ the initial position of material points $i$ in physical space and $\mathbf{x}_i = \varphi(\mathbf{X}_i) = \mathbf{X}_i + \mathbf{u}(\mathbf{X}_i)$ their position in the deformed state. Relevant measures for strain are the deformation gradient

$$\mathbf{F} = \nabla\varphi, \tag{1}$$

a second rank tensor that is generally not symmetric, and the symmetric Green strain tensor $\frac{1}{2}(\mathbf{F}^{\mathrm{T}}\mathbf{F} - \mathbf{U})$, where $\mathbf{U}$ denotes the unit tensor in 3D. With $J = \det(\mathbf{F})$ the Jacobian of $\mathbf{F}$, the stress measures of our analysis transform as follows:

$$\mathbf{S} = J\mathbf{F}^{-1}\boldsymbol{\sigma}\mathbf{F}^{-\mathrm{T}}, \tag{2}$$

$$\mathbf{P} = J\boldsymbol{\sigma}\mathbf{F}^{-\mathrm{T}}, \tag{3}$$

$$\mathbf{S} = \mathbf{F}^{-1}\mathbf{P}. \tag{4}$$

Consistency between the atomic-scale simulation and the continuum picture in our work requires agreement on the net mechanical work in configurations with a finite volume, for instance the DFT simulation cell and its representation in an equivalent continuum picture. This requirement touches upon yet another important issue, well recognized in studies of capillarity, namely the choice of a convention for locating the dividing surface S that defines the volume in the continuum description. A natural requirement for such a convention is that it ensures the referential volume enclosed by S to agree with the product of the number $N$ of atoms and the atomic volume $\Omega$ in the reference state. This specification is compatible with the mechanics in our work [31]. For planar and sufficiently symmetric crystal surfaces, the dividing surface is located halfway between the outermost lattice plane and the first missing plane. Care is required at curved surfaces, since inconsistent location of S may introduce artificial curvature-

dependencies of physical properties.

## 3. Effective elastic response – the continuum picture

### 3.1. Constitutive assumptions

We now derive the continuum description of a circular nanowire subjected to axial tension, bending, or torsion as illustrated in Fig. 1.

We analyze the mechanics of a finite solid body, restricting attention to linear elasticity and small strains. Our continuum approach is based on Refs [15,32]; it uses Lagrangian coordinates and describes the energetics in terms of a bulk free energy density (per volume) function $\Psi = \Psi(\mathbf{E})$ with strain tensor $\mathbf{E}$ and of a surface free energy density (per area) $\psi = \psi(\mathbb{E})$ with $\mathbb{E}$ the tangential strain tensor. The strain variable for the bulk is the Green strain tensor in the limit of small strain,

$$\mathbf{E} = \frac{1}{2}\left(\nabla\mathbf{u} + (\nabla\mathbf{u})^{\mathrm{T}}\right). \tag{5}$$

The local tangential strain at any point on the surface is a projection of the bulk strain near that point into the local surface plane,

$$\mathbb{E} = \mathbb{P}\mathbf{E}\mathbb{P}. \tag{6}$$

With $\mathbf{n}$ the local outer surface normal and $\otimes$ the Kronecker product, the local surface projection tensor $\mathbb{P}$ at any point on the surface is given by

$$\mathbb{P} = \mathbf{U} - \mathbf{n}\otimes\mathbf{n}. \tag{7}$$

Equation (6) connects the deformation at the surface to that of the bulk, thereby introducing the coherency constraint at the crystal surface into the continuum analysis.

The free energy densities are defined so that the net free energy $\mathfrak{F}$ combines a volume, $V$, integral over $\Psi$ in the bulk, B, and an area, $A$, integral over $\psi$ on the surface, S, as $\mathfrak{F} = \int_{\mathrm{B}} \Psi \mathrm{d}V + \int_{\mathrm{S}} \psi \mathrm{d}A$.

We work with linear elastic constitutive assumptions for the elastic response of the bulk and of the surface. Allowing for in-plane anisotropy of the surface—as in low-symmetry crystal faces—we take the equation of state for $\Psi$ and $\psi$ as

$$\Psi = \Psi_0 + \frac{1}{2}\mathbf{E}\cdot\mathbf{C}\cdot\mathbf{E}, \tag{8}$$

$$\psi = \psi_0 + \mathbb{S}_0\cdot\mathbb{E} + \frac{1}{2}\mathbb{E}\cdot\mathbb{C}\cdot\mathbb{E}, \tag{9}$$

respectively. $\mathbf{C}$ and $\mathbb{C}$ are fourth rank tensors representing the stiffness of the bulk and the excess stiffness of the surface [32]. The surface stress is denoted by $\mathbb{S}$, and specifically $\mathbb{S}_0$ is its value in the reference state. Thus, strain changes the bulk stress $\mathbf{S}$ and the surface stress $\mathbb{S}$ according to

$$\mathbf{S} = \frac{\mathrm{d}\Psi}{\mathrm{d}\mathbf{E}} = \mathbf{E}\cdot\mathbf{C}, \tag{10}$$

$$\mathbb{S} = \frac{\mathrm{d}\psi}{\mathrm{d}\mathbb{E}} = \mathbb{S}_0 + \mathbb{E}\cdot\mathbb{C}. \tag{11}$$

By their definition as derivatives of free energy densities in *referential* coordinates with respect to the small-strain limit of the Green strain given in Equation (5), $\mathbf{S}$ and $\mathbb{S}$ are 2nd Piola-Kirchhoff stresses.

In the interest of conciseness, our continuum analysis is restricted to isotropic solids. Here, we specify strain relative to a reference state which is stress-free (and isotropic, not sheared) in the bulk, and we express the elastic response of the bulk and of the surface in the form

$$\mathbf{S} = 2\mu^{\mathrm{B}}\mathbf{E} + \lambda^{\mathrm{B}}\mathrm{tr}(\mathbf{E})\mathbf{U}, \tag{12}$$

$$\mathbb{S} = f_0\mathbb{P} + 2\mu^{\mathrm{S}}\mathbb{E} + \lambda^{\mathrm{S}}\mathrm{tr}(\mathbb{E})\mathbb{P}. \tag{13}$$

The symbols have the following meaning: $f_0$: scalar surface stress parameter of the undeformed surface; $\mu$ and $\lambda$: Lamé constants for bulk or surface [15], as indicated by labels.

In experimental studies it is usual to characterize the *bulk* elastic response of isotropic solids in terms of Young's modulus $Y^{\mathrm{B}}$ and Poisson's ratio $\nu^{\mathrm{B}}$. For the convenience of the experimentalist, we will display selected results using this more familiar representation. The conversion rules are

$$\mu^{\mathrm{B}} = Y^{\mathrm{B}}\frac{1}{2(1+\nu^{\mathrm{B}})}, \quad \lambda^{\mathrm{B}} = Y^{\mathrm{B}}\frac{\nu^{\mathrm{B}}}{(1+\nu^{\mathrm{B}})(1-2\nu^{\mathrm{B}})}. \tag{14}$$

When exploring the elasticity of crystal surfaces, as in our DFT study, we allow for the elastic response to follow the symmetry of a cubic crystal. We define orthogonal surface principal directions $\mathbf{u}_1$ and $\mathbf{u}_2$, and we specify the independent components of $\mathbb{C}$ via Voigt notation (indices are contracted as $11 \to 1$, $22 \to 2$, $12 \to 4$). The relevant surface excess elastic parameters are $\mathbb{C}_{11}$, $\mathbb{C}_{12}$, and $\mathbb{C}_{44}$. For high symmetry surfaces, such as the (111) surface of gold [21], the elastic response is isotropic in the plane, and in that instance the two independent excess elastic parameters $\mathbb{C}_{11}$ and $\mathbb{C}_{12}$ relate to the surface Lamé constants through

$$\mu^{\mathrm{S}} = \frac{1}{2}(\mathbb{C}_{11} - \mathbb{C}_{12}) = \mathbb{C}_{44} \quad \text{and} \quad \lambda^{\mathrm{S}} = \mathbb{C}_{12}, \tag{15}$$

respectively.

### 3.2. Equilibrium conditions

The equilibrium condition for the stress in the bulk is

$$\mathrm{div}\,\mathbf{S} = 0, \tag{16}$$

whereas the local equilibrium at the surface in the absence of external load satisfies the Gurtin-Murdoch condition [15]

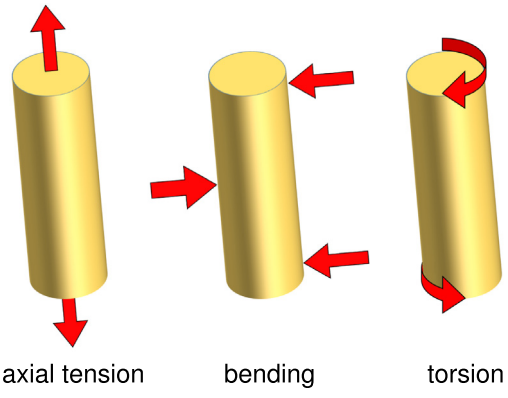


**Fig. 1.** Schematic illustration of a circular nanowire subjected to axial tension, bending, and torsion.

$$\mathbf{S}\cdot\mathbf{n} + \mathrm{div}_S\mathbb{S} = 0, \tag{17}$$

with $\mathrm{div}_S$ the surface divergence operator. This condition specifies the normal stress component at the surface. The remaining stress components are constrained by the Weissmüller-Cahn mean stress condition [19]. Assuming once more the absence of external load, this balance equation reads

$$\int_B \mathbf{S}\mathrm{d}V + \int_S \mathbb{S}\mathrm{d}A = 0. \tag{18}$$

Because of the superposition principle of linear elasticity, external loads and their compensating bulk stresses are simply additive to Equation (18).

### 3.3. Axial stiffness of a circular nanowire

Our analysis here considers a long (no end effects) cylinder of radius $r$ that is loaded exclusively by an external traction $T$ which acts along the axis. Symmetry requires the stress and the strain in the bulk to be uniform and isotropic in cross-sectional planes. Stress and strain are then completely specified by their axial and radial components, $S_A$ and $S_R$ for the stress and $E_A$ and $E_R$ for the strain. In matrix notation, using Cartesian coordinates, we thus have

$$\mathbf{E} = \begin{pmatrix} E_R & 0 & 0 \\ 0 & E_R & 0 \\ 0 & 0 & E_A \end{pmatrix}, \quad \mathbf{S} = \begin{pmatrix} S_R & 0 & 0 \\ 0 & S_R & 0 \\ 0 & 0 & S_A \end{pmatrix}. \tag{19}$$

Equation (16) is here automatically satisfied since $\mathbf{S}$ is uniform. Equation (17) requires for the *radial* stresses that

$$\frac{1}{r}\mathbf{t}\cdot\mathbb{S}\cdot\mathbf{t} + S_R = 0, \tag{20}$$

where $\mathbf{t}$ is a tangential unit vector in the surface plane, oriented normal to the nanowire axis. Specifically, $\mathbf{t} = \mathbf{a}\times\mathbf{n}$ with $\mathbf{a}$ the axial unit vector. Furthermore, Equation (18) along with the superposition principle of linear elasticity here implies for the *axial* stress

$$2\pi r\,\mathbf{a}\cdot\mathbb{S}\cdot\mathbf{a} + \pi r^2 S_A = \pi r^2 T. \tag{21}$$

Solutions for the stress and strain fields are readily found when accounting for the constitutive Equation (13) along with the above equilibrium conditions. If there is no surface excess elasticity, the stresses and strains at equilibrium scale linearly with the specific surface area (area per volume) $\alpha$ [19,33]. For the geometry under consideration we have $\alpha = 2/r$. Accounting for excess elasticity introduces higher order terms in $\alpha$ that are typically negligible in experimental situations unless the nanowire radius is exceedingly small. Therefore, and in the interest of conciseness, we take series expansions in $\alpha$ around $\alpha = 0$ for all results and we display only terms up to order $\alpha$.

In the absence of an external load, the stress and strain components are obtained as

$$S_A = -\alpha f_0 \quad \text{and} \quad S_R = -\frac{1}{2}\alpha f_0 \tag{22}$$

and

$$E_A = -\alpha f_0\frac{1-\nu^B}{Y^B} \quad \text{and} \quad E_R = -\alpha f_0\frac{1-3\nu^B}{2Y^B}. \tag{23}$$

The agreement with previous results for stress [19] and strain [33] supports the present analysis.

The effective Young's modulus $Y^{\mathrm{eff}}$ of the nanowire is obtained from the solution for the strain through

$$Y^{\mathrm{eff}} = \left(\frac{\mathrm{d}E_A}{\mathrm{d}T}\right)^{-1}. \tag{24}$$

To first order in $\alpha$ it is

$$Y^{\mathrm{eff}} = Y^B + \alpha\left(\lambda^S\left(1-\nu^B\right)^2 + 2\mu^S\left(1+\left(\nu^B\right)^2\right)\right). \tag{25}$$

In terms of the excess elasticity coefficients $\mathbb{C}_{ij}$, this result reads

$$Y^{\mathrm{eff}} = Y^B + \alpha\left(\mathbb{C}_{11}\left(1+\left(\nu^B\right)^2\right) - 2\mathbb{C}_{12}\nu^B\right). \tag{26}$$

This result agrees with the previous computation in [34], and the agreement again supports our analysis.

### 3.4. Torsion stiffness of a circular nanowire

Consider a wire of length $L$ and twisted through an angle $\phi$ about its axis, so that the strain is

$$\mathbf{E} = \frac{\rho\phi}{2L}\begin{pmatrix} 0 & 0 & \sin\theta \\ 0 & 0 & -\cos\theta \\ \sin\theta & -\cos\theta & 0 \end{pmatrix}, \tag{27}$$

with $\rho$ the radial distance from the wire's central axis and $\theta$ a polar angle in the cross-sectional plane.

The bulk strain $\mathbf{E}$ of Equation (27) is a pure shear, and the same holds for the tangential strain $\mathbb{E}$ at the surface. By virtue of Equation (13), the tangential strain adds a shear component $\Delta\mathbb{S}$ to the surface stress. This extra surface stress depends only on $\mu^S$ and not on $\lambda^S$. Furthermore, the extra stress does not affect the normal stress balance of Equation (17). In other words, the surface excess elasticity does not affect the stress or strain in the bulk of the twisted nanowire at equilibrium. Equation (27) is then exact and may be used, along with the projection Equation (6) and the stress-strain relations (12) and (13), to compute the torque $\widehat{T}$ through

$$\widehat{T} = \int_0^r\int_0^{2\pi}\mathbf{t}\cdot\mathbf{S}\cdot\mathbf{a}\rho\mathrm{d}\theta\mathrm{d}\rho + \int_0^{2\pi}\mathbf{t}\cdot\mathbb{S}\cdot\mathbf{a}r\mathrm{d}\theta. \tag{28}$$

The result is

$$\widehat{T} = \widehat{J}\frac{\phi}{L}\left(G^B + 2\alpha\mu^S\right), \tag{29}$$

with $\widehat{J} = \pi/2r^4$ the polar moment of area of the wire cross-section and $G^B = \frac{1}{2}Y^B/(1+\nu^B)$ the shear modulus in the bulk. As the torsional rigidity of a beam is defined as the product of $\widehat{J}$ and the shear modulus, Equation (29) suggests that the torsional rigidity of a nanowire is $\widehat{J}G^{\mathrm{eff}}$, with the effective shear modulus given by

$$G^{\mathrm{eff}} = G^B + 2\alpha\mu^S = G^B + 2\alpha\mathbb{C}_{44}. \tag{30}$$

### 3.5. Bending stiffness of a circular nanowire

Here, we consider the load conditions required for bending the circular nanowire to a bending curvature $\kappa$. In the absence of

surface stress and surface-induced relaxation, the strain is then

$$\mathbf{E} = \kappa x \begin{pmatrix} -\nu^{\mathrm{B}} & 0 & 0 \\ 0 & -\nu^{\mathrm{B}} & 0 \\ 0 & 0 & 1 \end{pmatrix}, \tag{31}$$

with $x$ the distance from the neutral fiber.

If a wire with surface stress is bent, the capillary forces are no longer uniform and Equation (20) requires extra bulk stress components for compensation. In other words, on top of the bending strain of Equation (31), a nonuniform elastic relaxation in the wire is required. This may affect the bending moment. We have not found a closed-form solution for the relaxation. However, one may—in a Voigt-type scenario—ignore the relaxation and obtain an approximate solution as an upper limit of the bending stiffness. This amounts to assuming that the leading contribution of the surface stress to the bending moment is simply due to the axial forces that result when the bending strain field of Equation (31) modifies the surface stress through Equation (13). The bending moment is here obtained from

$$M = \int_{\mathrm{C}} \mathbf{a}\cdot\mathbf{S}\cdot\mathbf{a}\, x \mathrm{d}s + \int_{\mathrm{P}} \mathbf{a}\cdot\mathbb{S}\cdot\mathbf{a}\, x \mathrm{d}l, \tag{32}$$

with $s$ an area element on the cross-sectional surface C of the wire and $l$ a line element on its perimeter P. The result is

$$M = \frac{\pi}{4} r^4 \kappa Y^{\mathrm{B}} + \pi r^3 \kappa \left(\lambda^{\mathrm{S}}\left(1-\nu^{\mathrm{B}}\right) + 2\mu^{\mathrm{S}}\right). \tag{33}$$

Our approximate result for the bending stiffness K of the circular nanowire with surface excess elasticity is therefore $K = \pi/4 r^4 Y^{\mathrm{eff}}$, with the effective Young's modulus for bending given by

$$Y^{\mathrm{eff}} = Y^{\mathrm{B}} + 2\alpha\left(\lambda^{\mathrm{S}}\left(1-\nu^{\mathrm{B}}\right) + 2\mu^{\mathrm{S}}\right), \tag{34}$$

or equivalently

$$Y^{\mathrm{eff}} = Y^{\mathrm{B}} + 2\alpha\left(\mathbb{C}_{11} - \nu^{\mathrm{B}}\mathbb{C}_{12}\right). \tag{35}$$

To summarize, Equations (26), (30) and (35) express the impact of the surface on the effective elastic response of nanowires as products of the specific surface area and combinations of the surface excess stiffness tensor components $\mathbb{C}_{ij}$.

### 3.6. Impact of the reference state for strain

As outlined in Section 2, our continuum analysis is formulated in terms of 2nd Piola-Kirchhoff stresses whereas experiments typically work with 1st Piola-Kirchhoff stresses. This raises the question, how can our continuum expressions for $Y^{\mathrm{eff}}$ be compared to experimental values.

To clarify the issue, we have used the conversion rule of Equation (4), considering the strain of Equation (19), which allows to express the external traction $T$ in Equation (21) in terms of the 1st Piola-Kirchhoff (or "engineering") external applied stress $\tau^{\mathrm{eng}}$ as $T = \tau^{\mathrm{eng}}(1 - E_{\mathrm{A}})$. The experimental measure for $Y^{\mathrm{eff}}$ is obtained by again solving for the stresses at equilibrium and then taking the derivative in Equation (24) with respect to $\tau^{\mathrm{eng}}$ as opposed to $T$. If the experimental strain is measured relative to the *relaxed* state of the nanowire, where the internal stresses and strains are already equilibrated with the surface stress $f_0$ but where no external load acts as yet, then Equations (25) and (26) do provide the correct description of the experimental stress-strain response. This definition of strain is indeed a natural one in experiment.

We have applied similar checks to the torsion and bending stiffness results above. The situation is more benign since symmetry considerations forbid torsion or bending contributions to the relaxation in the absence of an external load. Furthermore, one readily finds that $T = \tau^{\mathrm{eng}}$ for torsion; therefore the choice of the experimental reference state is of no consequence. We also find that differences between the bending moments in the 2nd versus the 1st Piola-Kirchhoff representation depend on the bending curvature with $\kappa^2$ in leading order. Here again, the effective elastic coefficient derived in our continuum analysis can be directly transferred to the experimental reference frame.

## 4. Ab initio calculation of surface excess elasticity

### 4.1. Computational

For the Density Functional Theory (DFT) calculations, we employed the Vienna Ab initio Simulation Package (VASP) [35–38], its implemented projector-augmented wave (PAW) potentials [39,40], and the local density approximation (LDA) [41]. First-order Methfessel-Paxton [42] smearing was applied with a smearing width of 0.4 eV. Whenever required, ionic positions were relaxed until all force components were smaller than $5{\cdot}10^{-5}$ eVÅ$^{-1}$.

Surfaces were modeled by 12-layer fcc surface slabs in (111) and (001) orientation, containing one atom per atomic layer parallel to the surface. Convergence with respect to the number of atomic layers was carefully tested, and no significant impact on the surface excess elastic parameters was found. In order to avoid interaction between periodic images of the surfaces, 15 Å of separating vacuum were added to the equilibrium dimension of the surface slabs. All surface energy densities and stresses were calculated with reference to the smallest possible bulk cell of the same orientation and mixed boundary conditions.

All results were checked for convergence with respect to smearing, $k$-point sampling, and energy cutoff, and details are provided in the supplementary online material. For surface and bulk calculations, the same in-plane grid of Monkhorst-Pack [43] $k$-points was used. In case of surface cells, a single $k$-point was used for the long cell direction. The number of $k$-points in the long direction of the bulk cells was chosen to approximately match the $k$-point density of the lateral directions. All presented calculations were performed with the highly increased energy cutoff of 1100 eV.

The equilibrium lattice constant was calculated for the (111) and (001) bulk reference cells via a Murnaghan fit. Bulk elastic parameters $C_{ij}$ were obtained via the stress-based routine [44] implemented in VASP, involving stress-based optimization of the cell dimensions as recommended by Caro et al. [45]. Results for relevant bulk properties are presented in Table 1, and the excellent agreement to other computational and experimental data supports our analysis.

### 4.2. Calculation of surface energy and surface stress

The surface stress of the unstrained (111) and (001) surfaces is isotropic, so that we can specify it by the scalar surface stress variable $f_0$ (see Section 3). The surface excess elastic parameters are subject to symmetry constraints [21,22], so that the (111) surface of the fcc lattice is characterized by only three non-zero surface excess elastic parameters, two of which are independent ($\mathbb{C}_{11}$, $\mathbb{C}_{12}$, $2\mathbb{C}_{44} = \mathbb{C}_{11} - \mathbb{C}_{12}$). In case of the (001) surface, three non-zero independent surface excess elastic parameters need to be considered ($\mathbb{C}_{11}$, $\mathbb{C}_{12}$, $\mathbb{C}_{44}$). The principal surface directions $\mathbf{u}_1$ and $\mathbf{u}_2$ correspond to the $[1\bar{1}0]$ and $[11\bar{2}]$ directions of the (111) surface and to the [100] and [010] directions of the (001) surface, respectively.

To probe the strain-dependence of surface energy and surface stress, we applied alternatively the uniaxial tangential deformation $\mathbf{F}^{(1)}$ and the tangential shear deformation $\mathbf{F}^{(2)}$ represented by the following deformation gradients:

$$\mathbf{F}^{(1)} = \begin{pmatrix} 1+\varepsilon & 0 & 0 \\ 0 & 1 & 0 \\ 0 & 0 & 1+\beta \end{pmatrix}, \quad \mathbf{F}^{(2)} = \begin{pmatrix} 1 & \gamma & 0 \\ \gamma & 1 & 0 \\ 0 & 0 & 1+\beta \end{pmatrix}. \tag{36}$$

The strain magnitudes $\varepsilon$ and $\gamma$ were restricted to the interval −0.015 to +0.015 so as to ascertain a linear elastic response of the surfaces.

Each desired tangential deformation was imposed on the initially unstrained (111) and (001) bulk cells. As the mixed boundary conditions of the surface require the crystal to be stress-free in direction of the surface normal **n**, the corresponding bulk contraction was found by minimizing the total energy of the tangentially strained bulk cells with respect to the normal strain parameter $\beta$.

Starting configurations for the surface slabs were constructed with tangential strain and bulk contraction identical to that of the corresponding bulk reference. On each side of the slab, the five outer surface layers were allowed to relax to their new equilibrium positions—leaving only the central two layers fixed with contracted bulk interlayer spacing.

The surface energy density $\psi$ was calculated as

$$\psi = \frac{1}{2A_0}\left[\mathscr{E}^{\text{slab}} - \left(N^{\text{slab}}\middle/N^{\text{bulk}}\right)\mathscr{E}^{\text{bulk}}\right] \tag{37}$$

where $\mathscr{E}^{\text{slab}}$ and $\mathscr{E}^{\text{bulk}}$ denote the total energies of surface and bulk cells (subjected to the same mixed boundary conditions) containing $N^{\text{slab}}$ and $N^{\text{bulk}}$ atoms, respectively. Equation (37) is consistent with the remarks in Section 3.1 on locating the dividing surface: Since the reference configuration is the stress-free periodic crystal lattice, the atomic volume has a given, constant value and so the comparison of the slab properties to a bulk reference with the same number of atoms ensures that the reference state also has the same Lagrangian volume as the slab.

As first presented by Needs [51], the *Cauchy* surface stress follows directly from the DFT stress tensor as

$$\mathbb{o}_i = \frac{1}{2A}\left[V^{\text{slab}}\sigma_i^{\text{slab}} - \left(N^{\text{slab}}\middle/N^{\text{bulk}}\right)V^{\text{bulk}}\sigma_i^{\text{bulk}}\right], \tag{38}$$

where $\sigma_i^{\text{slab}}$ and $\sigma_i^{\text{bulk}}$ denote the entries of the DFT stress tensor of surface and bulk cells with current, deformed cross section $A$ and volumes $V^{\text{slab}}$ and $V^{\text{bulk}}$ respectively. As for the surface energy density, surface and bulk cells are subjected to the same mixed boundary conditions.

Our continuum analysis employs Lagrangian coordinates, and we emphasize the need for consistency between both approaches. This is relevant here, since the DFT code exclusively considers the current configuration provided to the simulation and so yields Cauchy stresses. The distinction is irrelevant if only the surface stress in the reference configuration is of interest, since in this case the actual and reference configuration are identical. By contrast, strain derivatives of the surface stresses—as required in our scheme for evaluating surface excess elastic parameters—differ between the Cauchy and Lagrangian descriptions. Accordingly, we obtain the Lagrangian surface stress via the transformation (2) as

**Table 1**
Lattice constant $a_0$ and bulk elastic parameters $C_{ij}$ of Au in comparison to other computational and experimental results.

| | This work | Computational | | Experimental | |
|---|---|---|---|---|---|
| $a_0$ (Å) | 4.0516 | 4.07[a] | 4.066[b] | 4.072[c] | 4.078[e] |
| $C_{11}$ (GPa) | 211 | 202.1[a] | 201.3[b] | 200.4[d] | 191[e] |
| $C_{12}$ (GPa) | 183 | 174.2[a] | 176.1[b] | 169.5[d] | 162[e] |
| $C_{44}$ (GPa) | 37 | 37.9[a] | 36.9[b] | 44.5[d] | 42.2[e] |

[a] USPP, GGA: Ref [46].
[b] FP-LMTO, LDA: Ref [47].
[c] X-ray diffraction, 293 K: Ref [48].
[d] Torsional-bar-resonance, 79 K: Ref [49].
[e] Ref [50].

$$\mathbb{S}_i = \frac{1}{2A_0}\left[V_0^{\text{slab}}S_i^{\text{slab}} - \left(N^{\text{slab}}\middle/N^{\text{bulk}}\right)V_0^{\text{bulk}}S_i^{\text{bulk}}\right], \tag{39}$$

where $S_i^{\text{slab}}$ and $S_i^{\text{bulk}}$ mark the required entries of the 2nd Piola-Kirchhoff stress tensors of the surface and bulk cells, respectively. In the supplementary online material, we provide component-wise expressions for the required $\mathbb{S}_i$ in terms of the Cauchy stresses $\sigma_i$ and strain increments $\varepsilon$ and $\gamma$. Note that via Equations (38) and (39) we base our evaluation on stress calculations both defined with DFT-based values rather than using a continuum mechanics transformation.

### 4.3. Surface mechanical properties

The surface energy density $\psi_0$ and the surface stress $f_0$ (in the undeformed state $f_0 = \mathbb{o}_1 = \mathbb{S}_1$) were calculated according to Equations (37) and (39), respectively. Numerical values are presented in Table 2.

Surface stress and surface excess elastic parameters were evaluated directly via the DFT stress tensor (see Equations (38) and (39)), as this approach was found substantially more robust than taking strain derivatives of the surface energy density. Calculation of the surface stress $\mathbb{o}_1$ as the difference between the entries of the slab and bulk stress tensors is exemplarily illustrated in Fig. 2 for the case of Au(111) under uniaxial tangential strain in the current configuration, using the axial component of the Euler strain. It is clearly visible that the stress strain response of the surface slab is dominated by the bulk contribution, resulting in only a slight negative slope of the surface stress with strain. Due to the dominating bulk influence, particularly precise values of the surface stress are required in order to evaluate the surface excess elastic parameters.

Fig. 3 shows the surface stress components as function of the surface tangential strain for both the Eulerian and Lagrangian frames of reference. As our DFT study is not inherently limited to small strain, we display the Cauchy surface stress components $\mathbb{o}_i$ as function of the corresponding entries of the Euler strain $\frac{1}{2}(\mathbf{U}-(\mathbf{F}\mathbf{F}^{\mathrm{T}})^{-1})$, while axial and shear components of the Green strain tensor $\frac{1}{2}(\mathbf{F}^{\mathrm{T}}\mathbf{F}-\mathbf{U})$ provide the abscissa values for the display of the Lagrangian surface stress components $\mathbb{S}_i$. The variation of the surface stress components with strain is well resolved, so that linear regression affords meaningful results for the linear elastic behavior of the surface, as embodied in the surface excess elastic parameters $\mathbb{c}_{11}$, $\mathbb{c}_{12}$, and $\mathbb{c}_{44}$ in the current configuration and $\mathbb{C}_{11}$, $\mathbb{C}_{12}$, and $\mathbb{C}_{44}$ in the Lagrangian frame of reference. While the degree of convergence is responsible for deviations of individual data points, we have found that the general magnitude of the change of surface stress remains stable over a wide range of $k$-grids and cutoffs. As presented in the supplementary online material, we expect the surface excess elastic parameters to change by less than

**Table 2**
Surface mechanical properties of Au(111) and Au(001). Surface energy $\psi_0$ ($Jm^{-2}$) and surface stress $f_0$ ($Nm^{-1}$) do not depend on the frame of reference. Surface excess elastic parameters are presented in Lagrangian coordinates, $\mathbb{C}_{ij}$ ($Nm^{-1}$), and in the current configuration, $\mathfrak{c}_{ij}$ ($Nm^{-1}$).

| | | $\psi_0$ | $f_0$ | $\mathbb{C}_{11}$ | $\mathfrak{c}_{11}$ | $\mathbb{C}_{12}$ | $\mathfrak{c}_{12}$ | $\mathbb{C}_{44}$ | $\mathfrak{c}_{44}$ |
|---|---|---|---|---|---|---|---|---|---|
| Au(111) | This work | 1.125 | 3.624 | −4.33 | −0.71 | 0.07 | −3.56 | −2.20[a] | 1.43[a] |
| | LDA[b] | 1.114 | 3.317 | – | – | – | – | – | – |
| | PBE[c] | 0.707 | 1.766 | – | – | – | – | – | – |
| | EAM[d] | 0.70 | 1.64 | −8.0 | – | −2.7 | – | −2.6 | – |
| Au(001) | This work | 1.342 | 2.883 | −2.91 | −0.03 | 0.62 | −2.27 | −2.08 | 3.68 |
| | LDA[b] | 1.343 | 2.723 | – | – | – | – | – | – |
| | PBE[c] | 0.864 | 2.073 | – | – | – | – | – | – |
| | EAM[d] | 0.80 | 1.41 | −5.3 | – | −2.5 | – | −4.0 | – |

[a] $\mathbb{C}_{44} = \frac{1}{2}(\mathbb{C}_{11} - \mathbb{C}_{12})$, $\mathfrak{c}_{44} = \frac{1}{2}(\mathfrak{c}_{11} - \mathfrak{c}_{12})$.
[b] Mixed basis PP, LDA, $a_0 = 4.085$ Å: Ref [52].
[c] PAW, PBE, $a_0 = 4.1740$ Å: Ref [53].
[d] Embedded Atom Method (EAM): Ref [21].

0.06 $Nm^{-1}$ upon an increase of cutoff or *k*-sampling. Accordingly, the here achieved numerical accuracy is considered sufficient, and the results provide a reliable set of first-principles surface excess elastic parameters. The surface excess elastic parameters for both frames of reference are listed in Table 2. We note that the numerical values in the Eulerian frame of reference may differ from those in the Lagrangian description due to the deformed reference. Parameters can readily be transferred between both frames of reference by considering the underlying deformations, yielding e.g. the relation $\mathfrak{c}_{11} = \mathbb{C}_{11} + f_0$.

Let us now asses our findings in relation to the state of the art. The numerical magnitude of the surface excess elastic parameters emerges in the order of a few $Nm^{-1}$, comparable to the numerical value of the surface stresses (see Table 2). In so far, our results agree with previous reports based on numerical studies with empirical (Embedded Atom Method, EAM) interatomic potentials. Yet, as discussed below, the signs of our $\mathbb{C}_{12}$ coefficients are opposite to what EAM predicts. The empirical potentials of previous studies have only limited transferability, and hence their applicability to the special case of surface excess elasticity has not been demonstrated. Our study follows a more rigorous approach, using DFT as a method that can be expected to provide more substantiated insights. As the present results have the considerably more substantiated basis they should be preferred over earlier reports.

In the introduction, we have pointed out that the state of the art from experiments establishes no general trend for either, stiffening or softening of nanoscale objects by surface excess elasticity. Therefore it is necessary to carefully assess the reliability of the DFT surface excess elastic parameters on theoretical grounds. As a fist indicator, we consider the consistency of our calculations. Conceptionally, strain derivatives of the surface energy density (see Equation (9)) and the surface stress (see Equation (11)) are expected to yield identical results. However, differences can arise due to the computational implementation of total energy and stress [45]. Our analysis of the first strain-derivative of the surface energy density $\psi$ yields the surface stress $f_0$ in close agreement (Au(111): $f_0 = 3.617$ $Nm^{-1}$, Au(001): $f_0 = 2.870$ $Nm^{-1}$) to the direct calculation via the DFT stress tensor (see Table 2). This supports the consistency of both approaches and, thereby, the validity of our analysis.

As a second indicator, we compare our results to other theory data derived from LDA (local density approximation) and the PBE (Perdew-Burke-Enzerhof) functional. Table 2 shows that for both surface orientations, the surface energy density $\psi_0$ and surface stress $f_0$ agree well with literature LDA results. The two LDA potentials used in the present work and by Umeno et al. [52] yield larger surface energy densities $\psi_0$ and surface stresses $f_0$ than the PBE potential used by Zólyomi et al. [53]. However, we note that the PBE potential also strongly overestimates the experimental lattice parameter, while this is not the case for LDA (PBE: +2.4%; LDA: −0.6%). Hence, we conclude that the LDA potential yields the more accurate results for the surface stress. The EAM surface energy densities and surface stresses of Ref [21] are closer to the PBE values than to LDA. Yet, the EAM reproduces the same hierarchy of surface stresses as both LDA studies: $f_0^{(111)} > f_0^{(001)}$.

Finally, we compare our DFT results to the available experimental data for the bulk elastic parameters. It is well-known that DFT bulk elastic parameters may deviate from the corresponding experimental values in the order of ±10% [54–56]. A comparable deviation is found between the various potentials employed for the surface excess elastic parameters of ZnO, AlN, and GaN [25]. Our DFT elastic parameters for the bulk reproduce the experimental bulk elastic parameters with good accuracy (see Table 1). This emphasizes that the sign as well as the trends for the magnitude of the surface *excess* elastic parameters should also reliably emerge from DFT. We conclude that our observation of a *more compliant* behavior of the surface regions, that is embodied in the mainly *negative-valued* surface excess elastic parameters, is a robust and reliable finding. In view of the superiority of our DFT approach over previous studies using empirical potentials, we conclude that our results—which study the Au(111) and Au(001) surfaces as examples—yield the first reliable assessment of the elastic response of a metallic surface.

## 5. Effective elastic response of a circular nanowire

Let us now assess the implications of the DFT results for the effective stiffness of nanoscale objects. By using the DFT-based surface excess elastic parameters of Table 2 along with the continuum analysis of Section 3, we here combine insights from an atomic-scale model, in which the surface affects the local material's behavior in a region of finite thickness, with insights from a description in terms of an excess free energy function that applies to a two-dimensional surface. It is emphasized that the two approaches are in no way contradictory. As a phenomenological approach, the continuum picture is stringent provided that (1) the net excess energy of the solid body, per area, is correctly represented by the surface free energy function $\psi$ and that (2) the state variables are correctly identified [57]. The net energy of the atomic-scale model is known within the accuracy of the DFT, and our definitions of the location of the dividing surface provide meaningful values for the surface area as well as for the volume; the latter in turn implies a meaningful identification of the reference energy. This supports the adequacy of the numerical values for $\psi$

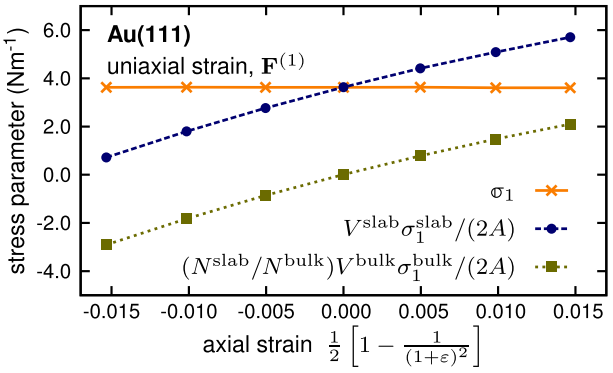


**Fig. 2.** Quantities entering the computation of the surface stress on Au(111) under uniaxial tangential strain. According to Equation (38), the Cauchy surface stress $\varpi_1$ follows as the difference between the total stress contribution of the surface slab $V^{\rm slab}\sigma_1^{\rm slab}/(2A)$ and the corresponding bulk reference $(N^{\rm slab}/N^{\rm bulk})V^{\rm bulk}\sigma_1^{\rm bulk}/(2A)$.

derived from DFT. The use of tangential superficial tensors—that is, projections of the bulk strain into the local surface plane—as the state variables for the strain is rigorously implied by the continuum analysis of surface elasticity, Ref [15]. Furthermore, Refs [31] and [32] have shown that the state variables and balance equations of Ref [15]—which underlie our continuum analysis—apply even when relaxation in a surface layer of final thickness is allowed for, so that additional deformation modes are active at the atomic scale. These considerations support our analysis and specifically the relevance of a reduction of the complex atom-by-atom behavior of surfaces to the simple and powerful description in terms of excess quantities.

In our continuum model, we have chosen an isotropic representation of the solid elastic response in order to arrive at simple equations that match the restricted precision of the experimental database. Consistent with the restriction to isotropic elasticity, we approximate the bulk behavior by using the elastic parameters of polycrystalline gold, $Y^{\rm B} = 78$ GPa and $\nu^{\rm B} = 0.44$, and we use the $\mathbb{C}_{ij}$ of Au(111) as an in-plane isotropic surface. Fig. 4 inspects the results for the axial, torsion, and bending stiffness of a circular nanowire versus the wire diameter. Displayed are the relative changes, $Y^{\rm eff}/Y^{\rm B}-1$ or $G^{\rm eff}/G^{\rm B}-1$, in effective stiffness (Equations (26), (30), (35)). It is seen that the surface excess elasticity has the strongest effect on the torsion stiffness. This is expected, since torsion involves the largest deformation in the surface regions, so surfaces contribute particularly strongly to the stiffness. The effect is less pronounced in bending, since regions near the intersection of

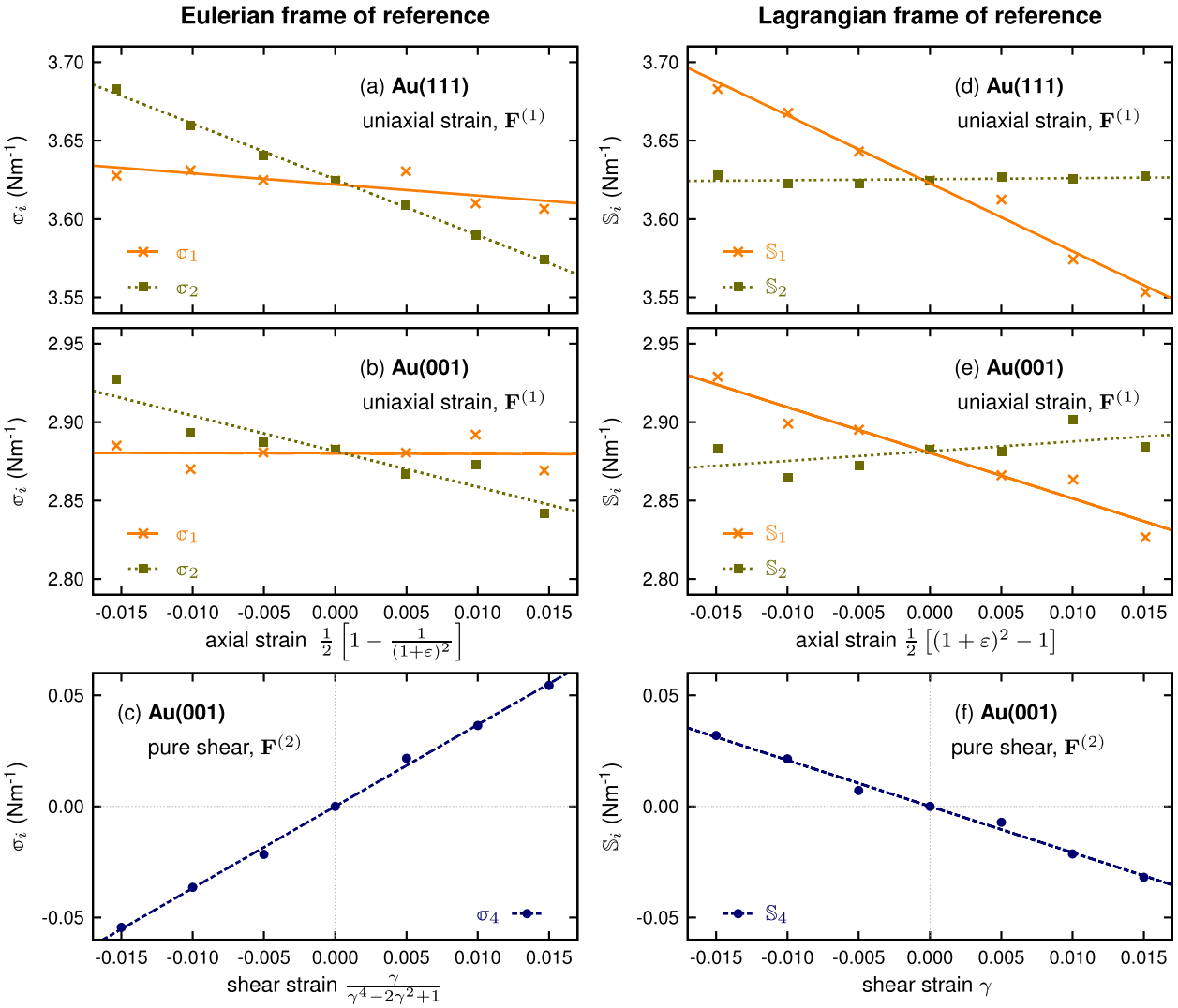


**Fig. 3.** Surface stress versus surface tangential strain. Figures (a)–(c) show the Cauchy surface stress $\varpi$ versus the Euler strain $\frac{1}{2}(\mathbf{U}-(\mathbf{F}\mathbf{F}^{\rm T})^{-1})$ within the Eulerian frame of reference, while Figures (d)–(f) show the 2nd Piola-Kirchhoff surface stress $\mathbb{S}$ versus the Green strain $\frac{1}{2}(\mathbf{F}^{\rm T}\mathbf{F}-\mathbf{U})$ within the Lagrangian frame of reference. Lines show linear fits to the data.

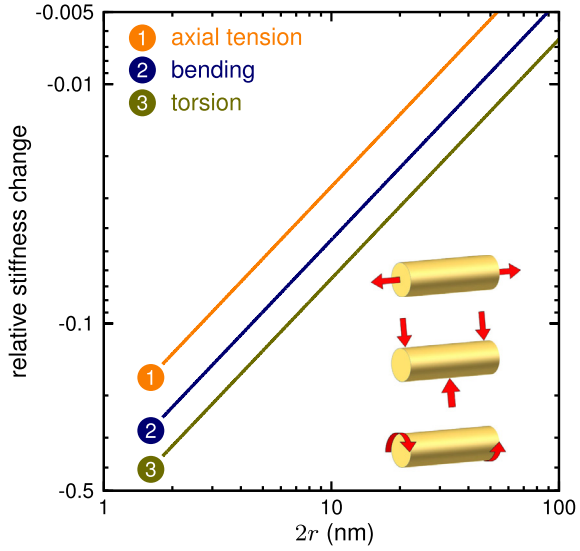


**Fig. 4.** Relative change, $Y^{eff}/Y^{B}-1$ or $G^{eff}/G^{B}-1$, in effective stiffness due to surface excess elasticity versus the nanowire diameter $2r$. Colors distinguish the three different deformation modes axial tension, bending, and torsion. Numerical values were used as indicated in the text. (For interpretation of the references to colour in this figure legend, the reader is referred to the web version of this article.)

the neutral fiber with the surface are not deformed at all and so do not contribute to the effective stiffness. The surface effect on axial deformation is least, because the transverse contraction (which is particularly pronounced in gold) implies that the surface deformation in the direction normal to the load axis is much smaller than the deformation along the load axis. Therefore, the overall deformation of the surface is less than the net change in length, implying less contribution of the surface regions to the axial stiffness.

It is also seen that the numerical values are such that only extremely small nanostructures are expected to respond to surface excess elasticity with measurable changes of the effective elastic response. For nanowires with diameters as small as 10 nm, and for wires with any larger diameter, the impact of the surface is at most in the order of a few percent, well below the detection limit in current experimental techniques. This statement also applies to an experimental issue that we briefly addressed in the introduction: surface excess elasticity has been discussed as one out of several possible explanations for the strong (one order of magnitude change) variation of the effective elasticity of nanoporous gold if the ligament diameter is varied between 10 and 100 nm. The message of Fig. 4 in this respect is unambiguous: The surface excess elastic parameters are substantially too small for explaining the observation as a surface effect.

Studies of nanoporous gold however point towards a different and important issue in the context of experiments. Covering the surface with one monolayer of adsorbed oxygen increases the stiffness of nanoporous gold with a ligament size of 40 nm by 10% [6]. Inspection of Fig. 4 reveals that this requires the surface excess elastic parameters of oxygen-covered gold to be at least a factor 10 larger and of opposite sign than the numerical values of the present study. This implies that surface adsorbate coverage may have a decisive effect on experimental investigations of surface excess elasticity. The notion is well compatible with the large scatter in the relevant experimental data and with the first-principles results for ZnO, GaN, and AlN [24–26], highlighting the possible impact of surface contaminants on the available experimental results. This suggests that future DFT studies of oxygen-covered surfaces are of high interest.

## 6. Summary

Our study is motivated by experimental reports of modified effective elastic response at small size. We focus on the possible contribution of the surface excess elasticity to this phenomenon, ignoring other effects such as nonlinear bulk elastic response. The key results of this work are numerical estimates of the surface mechanical properties of two low index surfaces of gold, computed by Density Functional Theory (DFT). The calculations yield the first complete set of DFT parameters including surface energy density, surface stress, and surface excess elastic parameters for a metal surface. We find positive- as well as negative-valued surface excess elastic parameters. In combination, their impact on the effective elastic response of nanowires under various deformation modes is an enhanced compliance at small size.

Our expressions for the impact of the surface excess elasticity on the effective elastic response of a cylindrical nanowire also provide an assessment of the magnitude of the enhanced compliance. We show that the surface excess elasticity affects the effective elastic response by only a few percent, even for diameters as small as 10 nm. By magnitude and sign, the consequences of surface excess elasticity do not explain the experimentally observed size-dependent properties of metal nanostructures.

Besides revealing the magnitude and the consequences of the surface excess elasticity, our study also advertises a conceptional issue in defining and evaluating local elastic constants at surfaces. Experiment, continuum theory and atomistic model each use independent conventions for defining the stresses and/or the strains. Care is required in consistently using the appropriate definitions and in converting between excess elastic parameters determined by the individual methods. This is exemplified by our comparison of the Cauchy excess elastic parameters that emerge from the atomistic computation to the 2nd Piola-Kirchhoff parameters of our continuum model. The two data sets differ substantially in numerical value. The distinction has not always been appreciated in earlier work and deserves more attention in future studies.

## Acknowledgements

The authors gratefully acknowledge financial support from the German Research Foundation (DFG) via SFB 986 “M³”, projects B2, B3, and B6.

## Appendix A. Supplementary data

Supplementary data related to this article can be found at http://dx.doi.org/10.1016/j.actamat.2016.10.066.

## References

[1] A. Husain, J. Hone, H.W.C. Postma, X.M.H. Huang, T. Drake, M. Barbic, A. Scherer, M.L. Roukes, Nanowire-based very-high-frequency electromechanical resonator, Appl. Phys. Lett. 83 (6) (2003) 1240–1242.
[2] H. Liang, M. Upmanyu, H. Huang, Size-dependent elasticity of nanowires: nonlinear effects, Phys. Rev. B 71 (2005) 241403(R).
[3] M.T. McDowell, A.M. Leach, K. Gall, On the elastic modulus of metallic nanowires, Nano Lett. 8 (11) (2008) 3613.
[4] E. Mile, G. Jourdan, I. Bargatin, S. Labarthe, C. Marcoux, P. Andreucci, S. Hentz, C. Kharrat, E. Colinet, L. Duraffourg, In-plane nanoelectromechanical resonators based on silicon nanowire piezoresistive detection, Nanotechnology 21 (16) (2010) 165504.
[5] H.J. Jin, X.L. Wang, S. Parida, K. Wang, M. Seo, J. Weissmüller, Nanoporous Au-Pt alloys as large strain electrochemical actuators, Nano Lett. 10 (1) (2010) 187.
[6] N. Mameka, J. Markmann, H.-J. Jin, J. Weissmüller, Electrical stiffness modulation–confirming the impact of surface excess elasticity on the mechanics of nanomaterials, Acta Mater. 76 (2014) 272.
[7] S. Cuenot, C. Frétigny, S. Demoustier-Champagne, B. Nysten, Surface tension effect on the mechanical properties of nanomaterials measured by atomic

force microscopy, Phys. Rev. B 69 (2004) 165410.
[8] G.Y. Jing, H.L. Duan, X.M. Sun, Z.S. Zhang, J. Xu, Y.D. Li, J.X. Wang, D.P. Yu, Surface effects on elastic properties of silver nanowires: contact atomic-force microscopy, Phys. Rev. B 73 (2006) 235409.
[9] A. Mathur, J. Erlebacher, Size dependence of effective Young's modulus of nanoporous gold, Appl. Phys. Lett. 90 (6) (2007) 061910.
[10] L.Y. Chen, G. Richter, J.P. Sullivan, D.S. Gianola, Lattice anharmonicity in defect-free Pd nanowhiskers, Phys. Rev. Lett. 109 (2012) 125503.
[11] N. Mameka, K. Wang, J. Markmann, E.T. Lilleodden, J. Weissmüller, Nanoporous gold—testing macro-scale samples to probe small-scale mechanical behavior, Mater. Res. Lett. 4 (1) (2016) 27.
[12] X. Li, T. Ono, Y. Wang, M. Esashi, Ultrathin single-crystalline-silicon cantilever resonators: fabrication technology and significant specimen size effect on Young's modulus, Appl. Phys. Lett. 83 (15) (2003) 3081.
[13] S.G. Nilsson, X. Borrisé, L. Montelius, Size effect on Young's modulus of thin chromium cantilevers, Appl. Phys. Lett. 85 (16) (2004) 3555.
[14] L. Qiao, X. Zheng, Effect of surface stress on the stiffness of micro/nano-cantilevers: nanowire elastic modulus measured by nano-scale tensile and vibrational techniques, J. Appl. Phys. 113 (1) (2013) 013508.
[15] M. Gurtin, A.I. Murdoch, A continuum theory of elastic material surfaces, Archive Ration. Mech. Analysis 57 (4) (1975) 291.
[16] B. Wu, A. Heidelberg, J.J. Boland, Mechanical properties of ultrahigh-strength gold nanowires, Nat. Mater. 4 (7) (2005) 525.
[17] R.C. Cammarata, K. Sieradzki, Surface and interface stresses, Annu. Rev. Mater. Sci. 24 (1994) 215.
[18] G. Yun, H.S. Park, Surface stress effects on the bending properties of fcc metal nanowires, Phys. Rev. B 79 (2009) 195421.
[19] J. Weissmüller, J.W. Cahn, Mean stresses in microstructures due to interface stresses: a generalization of a capillary equation for solids, Acta Mater. 45 (5) (1997) 1899–1906.
[20] B.-N.D. Ngô, A. Stukowski, N. Mameka, J. Markmann, K. Albe, J. Weissmüller, Anomalous compliance and early yielding of nanoporous gold, Acta Mater. 93 (2015) 144.
[21] V.B. Shenoy, Atomistic calculations of elastic properties of metallic fcc crystal surfaces, Phys. Rev. B 71 (2005) 094104.
[22] R. Dingreville, J. Qu, A semi-analytical method to compute surface elastic properties, Acta Mater. 55 (2007) 141.
[23] L.G. Zhou, H. Huang, Are surfaces elastically softer or stiffer? Appl. Phys. Lett. 84 (11) (2004) 1940.
[24] J. Yvonnet, A. Mitrushchenkov, G. Chambaud, Q.-C. He, S.-T. Gu, Characterization of surface and nonlinear elasticity in wurtzite ZnO nanowires, J. Appl. Phys. 111 (2012) 124305.
[25] M.-T. Hoang, J. Yvonnet, A. Mitrushchenkov, G. Chambaud, First-principles based multiscale model of piezoelectric nanowires with surface effects, J. Appl. Phys. 113 (2013) 014309.
[26] J. Yvonnet, A. Mitrushchenkov, G. Chambaud, Q.-C. He, Finite element model of ionic nanowires with size-dependent mechanical properties determined by ab initio calculations, Comput. Methods Appl. Mech. Eng. 200 (2011) 614.
[27] N. Huber, R. Viswanath, N. Mameka, J. Markmann, J. Weissmüller, Scaling laws of nanoporous metals under uniaxial compression, Acta Mater. 67 (2014) 252.
[28] O.H. Nielsen, R.M. Martin, First-principles calculation of stress, Phys. Rev. Lett. 50 (9) (1983) 697.
[29] O. H. Nielsen, R. M. Martin, Stress in semiconductors: ab initio calculations on Si, Ge, and GaAs, Phys. Rev. B 32(6).
[30] J. Bonet, R.D. Wood, Nonlinear continuum mechanics for finite element analysis, Cambridge University Press, Cambridge; New York, NY, 2008.
[31] J. Weissmüller, D. Kramer, Balance of force at curved solid metal-liquid electrolyte interfaces, Langmuir 21 (10) (2005) 4592.
[32] M.E. Gurtin, J. Weissmüller, F. Larché, A general theory of curved deformable interfaces in solids at equilibrium, Philos. Mag. A 78 (5) (1998) 1093.
[33] J. Weissmüller, H.L. Duan, D. Farkas, Deformation of solids with nanoscale pores by the action of capillary forces, Acta Mater. 58 (1) (2010) 1.
[34] H.L. Duan, X. Yi, Z.P. Huang, J.J. Wang, A unified scheme for prediction of effective moduli of multiphase composites ith interface effects. Part I: theoretical framework, Mech. Mater. 39 (1) (2007) 81.
[35] G. Kresse, J. Hafner, *Ab Initio* molecular dynamics for liquid metals, Phys. Rev. B 47 (1) (1993) 558.
[36] G. Kresse, J. Hafner, *Ab initio* molecular-dynamics simulation of the liquid-metal-amorphous-semiconductor transition in germanium, Phys. Rev. B 49 (20) (1994) 14251.
[37] G. Kresse, J. Furthmüller, Efficiency of *ab-initio* total energy calculations for metals and semiconductors using a plane-wave basis set, Comp. Mat. Sci. 6 (1996) 15.
[38] G. Kresse, J. Furthmüller, Efficient iterative schemes for *ab initio* total-energy calculations using a plane-wave basis set, Phys. Rev. B 54 (1996) 11169.
[39] P.E. Blöchl, Projector augmented-wave method, Phys. Rev. B 50 (2) (1994) 17953.
[40] G. Kresse, D. Joubert, From ultrasoft pseudopotentials to the projector augmented-wave method, Phys. Rev. B 59 (3) (1999) 1758.
[41] J.P. Perdew, A. Zunger, Self-interaction correction to density-functional approximations for many-electron systems, Phys. Rev. B 23 (1981) 5048.
[42] M. Methfessel, A.T. Paxton, High-precision sampling for Brillouin-zone integration in metals, Phys. Rev. B 40 (1989) 3616.
[43] H.J. Monkhorst, J.D. Pack, Special points for Brillouin-zone integrations, Phys. Rev. B 13 (1976) 5188.
[44] Y. Le Page, P. Saxe, Symmetry-general least-squares extraction of elastic data for strained materials from *ab-initio* calculations of stress, Phys. Rev. B 65 (2002) 104104.
[45] M.A. Caro, S. Schulz, E.P. O'Reilly, Comparison of stress and total energy methods for calculation of elastic properties of semiconductors, J. Phys. Condens. Matter 25 (2013) 025803.
[46] H. Wang, M. Li, *Ab initio* calculations of second-, third-, and fourth-order eelastic constants for single crystals, Phys. Rev. B 79 (2009) 224102.
[47] T. Tsuchiya, K. Kawamura, Pressure effect on elastic properties of crystalline au, J. Chem. Phys. 116 (5) (2002) 2121.
[48] I.K. Suh, H. Ohta, Y. Waseda, High-temperature thermal expansion of six metallic elements measured by dilatation method and x-ray diffraction, J. Mater. Sci. 23 (1988) 757.
[49] S.N. Biswas, P.V. 't Klooster, N.J. Trappeniers, Effect of pressure on the elastic constants of noble metals, Phys. B 103 (1981) 235.
[50] W. Martienssen, H. Warlimont (Eds.), Springer handbook of condensed matter and materials data, Springer, Berlin Heidelberg, 2005.
[51] R.J. Needs, Calculations of the surface stress tensor at aluminum (111) and (110) surfaces, Phys. Rev. Lett. 58 (1) (1987) 53.
[52] Y. Umeno, C. Elsässer, B. Meyer, P. Gumbsch, M. Nothacker, J. Weissmüller, F. Evers, *Ab initio* study of surface stress response to charging, Europhys. Lett. 78 (1) (2007) 13001.
[53] V. Zólyomi, L. Vitos, S.K. Kwon, J. Kollár, Surface relaxation and stress for 5d transition metals, J. Phys. Condens. Matter 21 (2009) 095007.
[54] M. Ropo, K. Kokko, L. Vitos, Assessing the Perdew-Burke-Ernzerhof exchange-correlation density functional revised for metallic bulk and surface systems, Phys. Rev. B 77 (2008) 195445.
[55] G.I. Csonka, J.P. Perdew, A. Ruzsinszky, P.H.T. Philipsen, S. Lebègue, J. Paier, O.A. Vydrov, J.G. Ángyán, Assessing the performance of recent density functionals for bulk solids, Phys. Rev. B 79 (2009) 155107.
[56] K. Lejaeghere, V.V. Speybroeck, G.V. Oost, S. Cottenier, Error estimates for solid-state density-functional theory predictions: an overview by means of the ground-state elemental crystals, Crit. Rev. Solid State Mater. Sci. 39 (1) (2014) 1.
[57] H. Callen, Thermodynamics and an introduction to thermostatistics, Wiley, New York, 1985.